ELSEVIER

Journal of Nuclear Materials 241–243 (1997) 982–987

journal of nuclear materials

Investigation of plasma facing components and vacuum vessel in RFX

P. Sonato *, V. Antoni, M. Bagatin, W.R. Baker, S. Peruzzo, L. Tramontin, P. Zaccaria, G. Zollino

Padova Fusion Research Group (EURATOM–ENEA–CNR–Università di Padova) Istituto Gas Ionizzati – CNR, Corso Stati Uniti 4, 35127 Padua, Italy

Abstract

The first wall components of RFX have been investigated after three years of operation and four boronization processes. The main damage is due to arcs and localized erosion. 112 new reshaped tiles have been installed and the removed ones have been carefully analysed in order to evaluate the effects due to plasma interaction. A strong redeposition of carbon and boron has been observed near the most damaged tiles. The redeposition pattern exhibits toroidal and poloidal asymmetry in agreement with the plasma flow measured in the outer region. For the first time evidence of halo currents flowing from the plasma to the vacuum vessel has been observed and their value has been estimated.

Keywords: RFX; Reversed field pinch; Erosion and particle deposition

1. Introduction

RFX [1] has a metallic vacuum vessel made of Inconel 625® protected by 2016 graphite tiles [2]. The tiles are distributed in 72 toroidally equispaced rings and 28 rows along the poloidal direction. With the exception of the 9 mm interspacing between the tiles in both the poloidal and toroidal direction, the graphite tiles completely protect the metallic wall. The interspacings between the tiles in the poloidal direction are not aligned in order to avoid a preferential path for the plasma along the magnetic field, which is mainly poloidal at the edge.

In three years of operation about 5000 plasma shots have been performed with a pulse length shorter than 200 ms and a plasma current up to 900 kA [3,4]. The ohmic input power ranged between 15 to 50 MW depending on the plasma density.

In each pulse the magnetic configuration exhibited a stationary disturbance due to many MHD instabilities locked at the wall [5,6] with main periodicity $m = 1$, $n = 8$ and a toroidal extension of less or equal to 40°. This disturbance tended to take place preferentially at the insulated poloidal gaps of the stabilising aluminium shell [7] which closely surrounds the vacuum vessel. Due to the magnetic disturbance energy fluxes up to 200 Mw/m^2 [6,8], parallel to the magnetic field, were directly deposited on the first wall.

In Section 2 the status of the first wall after the visual inspection by CCD camera is reported. In Section 3 the graphite erosion is estimated and the redeposition pattern is discussed. In Section 4 evidence of halo currents is discussed and an estimate of their magnitude is given.

2. Status of the first wall

The first wall has been inspected by a remote handling system (RHS) [2] fitted with a CCD camera. Two inspections were performed, the first one in 1993 [8] and the second one in 1995 after ~5000 plasma shots and 4 boronization processes with trimethylboron [9]. They were

* Corresponding author. Tel.: +39-49 8295 037; fax: +39-49 8700 718; e-mail: sonato@pdigi3.igi.pd.cnr.it.

0022-3115/97/$17.00 Copyright © 1997 Elsevier Science B.V. All rights reserved.
PII S0022-3115(96)00644-7

limited to the regions of the poloidal gaps where the majority of the local perturbations occurred. The second inspection revealed more severe damage of the components due to the phenomena of plasma–wall interaction identified after the first inspection.

2.1. Status of the graphite tiles

The main phenomena observed on the surface of the tiles have been identified as arcing, erosion and redeposition. These phenomena are more pronounced in the regions near the two insulated poloidal gaps.

Unipolar arc tracks are visible on the tile surfaces including the graphite caps that protect the molybdenum keys. They are mainly aligned along the toroidal direction confirming that they occur during the RFP phase of the discharge when the magnetic field is almost poloidal. As shown in Fig. 1, the large number of superimposed arcs makes the surface very rough. The number of arc tracks on the surface of each tile depends on the poloidal and toroidal location of the tile; in the worst case the original surface is completely eroded. Only in the outer equatorial region it is possible to find tiles where a large portion of the surface is not eroded by arcs.

Localized erosions are evident at the edges of some tiles and graphite caps exposed to the superthermal electron flow along the poloidal direction [6,8] (Figs. 1 and 2). This erosion preferentially takes place on the graphite tiles located in the lower part of the vessel (Fig. 2a) at the two poloidal gaps.

A redeposition of a carbon–boron hydrogenated layer is observed both on the rear and front faces of the tiles (Fig. 1). The thickness of the redeposited film, deduced from the interference colours [10], varies up to ~ 1 μm on the back of the tiles. The maximum redeposition appears in correspondence to the areas of maximum localized erosion.

In the upper part of the vessel (Fig. 2b) erosion from unipolar arcs and redeposition appear to combine in such a way that it is difficult to discern the original graphite surface and the direction of the arc tracks.

2.2. Status of the vessel surface

The vacuum vessel surface that is not protected by the tiles shows damage correlated to those of the graphite tiles: In correspondence to the localized erosion in the lower part of the vessel, 'grooves' in the metal surface along the poloidal direction, consistent with the flow of superthermal electrons, are observed (Fig. 2a) with a maximum depth of 0.2 mm, measured with a potentiometric transducer installed on the RHS.

Coloured spots with black borders have been found in proximity with the local erosion of the graphite due to redeposition of carbon and boron coming from the locally eroded areas. These spots are concentrated in the lower and outer equatorial regions of the vessel.

In correspondence with the uniform erosion of the graphite, in the upper region of the vessel, the metallic surface is so rough (Fig. 2b) that it has not been possible to measure the depth by the potentiometric transducer. This phenomenon extends in both the poloidal and toroidal interspacings between the tiles.

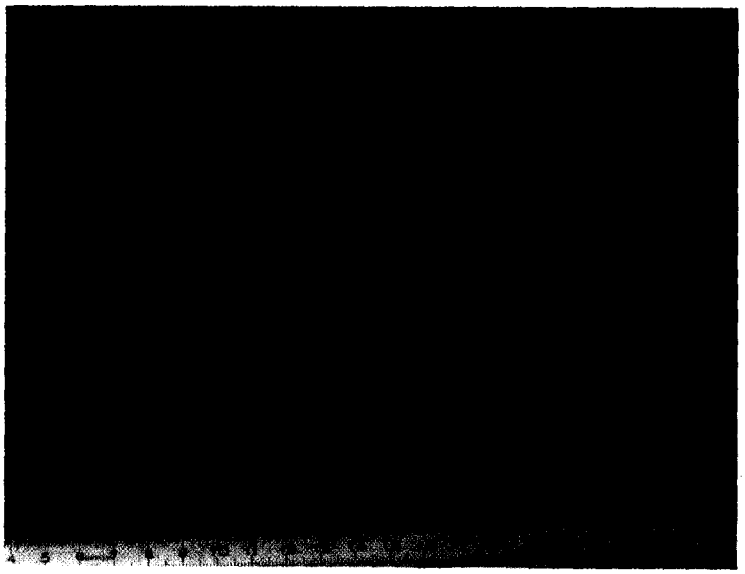

Fig. 1. Front and rear side of two neighbouring tiles substituted in 1995. The longer and shorter dimensions correspond to the toroidal and poloidal directions, respectively.

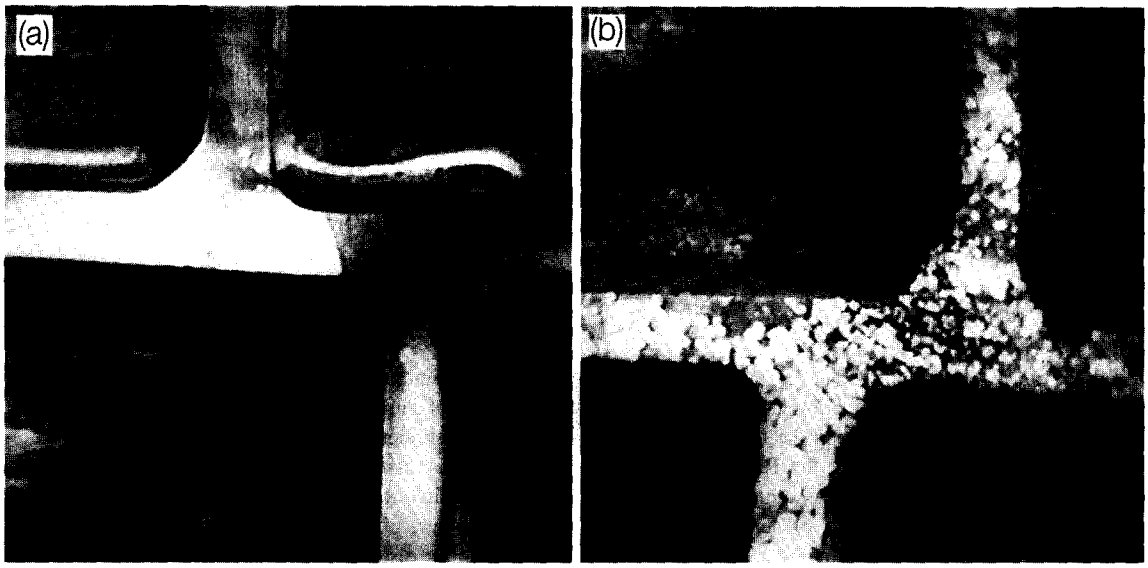

Fig. 2. Damage on the vessel surface and graphite tile edges in the poloidal gap region observed by means of the CCD camera installed on the RHS. The horizontal and vertical directions correspond to the toroidal and poloidal directions, respectively. (a) Lower part of the vessel. (b) Upper part of the vessel.

As for the graphite tiles all these phenomena are more pronounced in the region near the two insulated poloidal gaps.

3. Analysis of the graphite tiles

In order to completely protect the vacuum vessel at the gaps, during the last shut down in 1995, 112 graphite tiles have been substituted with new reshaped ones. The removed tiles have been analyzed to interpret the redeposition pattern and to estimate, for the worst cases, the localized erosion and redeposition thickness.

3.1. Measurement of localized erosion

After a detailed visual and photographic inspection, four of the tiles with the largest eroded areas were selected and a dimensional inspection was carried out to establish the extent of the erosion.

The dimensional inspection was carried out using a comparator (resolution 0.01 mm), microscope with an X–Y coordinate table (resolution 0.01 mm) and precise straight edges. As the eroded edge in its original form was radiused, the eroded section was taken as a tapered cylindrical section. To reduce the error as much as possible the area was divided into 36 sections and the volume calculated for each sector. The tile from the outer equatorial zone presents the greatest erosion and the quantity of material eroded from the main affected area is approximately 100 mm^3. In the previous inspection in 1993 the eroded material was estimated to be approximately 5 mm^3 per tile after about 1000 shots at low current [8]. Even taking into account the larger number of shots, the present erosion appears to be at least one order of magnitude larger, probably because of the higher current discharges during which carbon bloom phenomena were observed [11].

3.2. Boron analysis

Two graphite tiles located at one of the two poloidal gaps in a upper (U) and lower (L) part of the vessel have been analyzed in order to detect the boron concentration and its spatial distribution along the poloidal and toroidal coordinate. The surface analysis was performed using a 2.5 MeV Van de Graaff accelerator and boron was measured by means of the nuclear reaction $^{11}B(p, \alpha)^8Be$ with a 660 keV proton beam.

A local coordinate system was chosen with the x axis in the toroidal direction, the y axis in the poloidal one and with the origin at the corner of the graphite tiles exposed to the superthermal electron flow. The boron concentration on the front side along the poloidal direction (Fig. 3) increases by a factor of 5 going from the edge of the tile to its centre, confirming a severe erosion at the edge of the graphite exposed to the superthermal electrons [6,8]. It is worth noting that the areal density in the centre of the tile is in agreement with the quantity expected after 4 boronizations. The boron redeposition measured on the rear of the tiles varies along the poloidal direction and it is maximum near the most eroded areas. The redeposition thickness along the toroidal direction shows a decay length of about 9 mm independent on the poloidal coordinate.

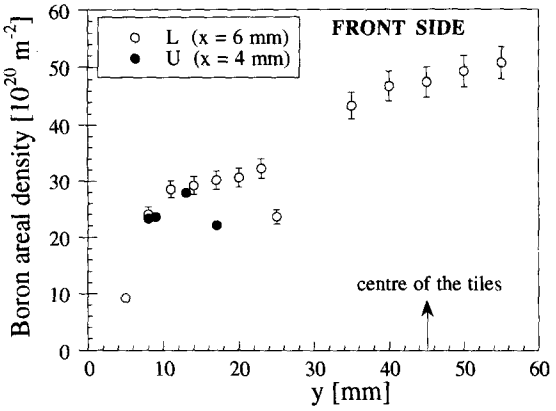

Fig. 3. Boron areal density measured on the front side of the tiles along the poloidal direction y.

3.3. Redeposition analysis

The inspection of the rear side of the 112 graphite tiles has revealed a non uniform redeposition of carbon and boron with a clear asymmetry in the toroidal direction with a maximum on the edge facing the ion diamagnetic drift. The toroidal extension of the redeposition, l_r, evidences a poloidal dependence for the tiles around the two poloidal gaps not affected by localized erosion (Fig. 4). The surface analysis of long term stainless steel samples exposed in the RFX scrape-off-layer has shown that the redeposited layer mainly consists of carbon. With this assumption, the analysis of the interference colours [10] indicates thickness values higher than 800 nm depending on the angle θ along the poloidal direction. The comparison with the local erosion of the tile edge confirms that most of the particles released by thermal erosion are redeposited locally [8].

The toroidal extension of the redeposition has been related to the carbon ion orbit through a simple expression, which takes into account the presence of a radial electric field in the outward direction. The electric field value is given by:

$$E = \frac{qB_\theta^2}{\pi m}\left[l_r \cdot \sqrt{1+\left(\frac{F}{\Theta}\right)^2} - r_L \cdot \left(1+\frac{F}{\Theta}\frac{\pi}{\sqrt{2}}\right)\right] \quad (1)$$

where F and Θ are the reversal and pinch parameters [1], B_θ is the magnetic field at the wall and r_L is the Larmor radius.

The redeposition asymmetry is consistent with the particle drift measured on RFX [12] which has been related to an ambipolar electric field which takes place in the outer region of RFP experiments. Taking an average temperature for the ions $T_i = 10$ eV (equal to the local electron temperature [8]), a poloidal magnetic field $B_\theta = 0.2$ T and $F/\Theta = 0.1$, the electric field in the outward direction ranges from 1 kV/m at the inner and outer equatorial location up to 2 kV/m at the top and bottom of the torus. The direction and value of the electric field is consistent with that measured by edge probes [13]. The asymmetry top–bottom versus in–outboard confirms that at the gap the plasma column is distorted.

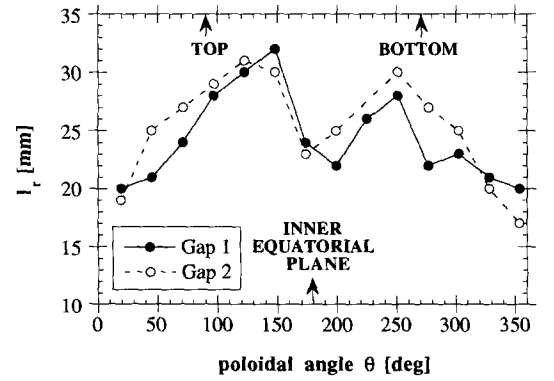

Fig. 4. Toroidal extension of the redeposition, l_r, as a function of the poloidal angle θ, on the rear side of the tiles along the two poloidal gaps.

4. Halo currents

During the investigation of the removed tiles and the inspection of the vacuum vessel in the gap regions, electric arcing and metal melting traces in the contact areas between graphite tiles and Inconel 625 stiffening rings have been observed (Fig. 1). These phenomena can be ascribed to the effects of halo currents, which flow partially in the plasma edge and partially in the first wall components and the vacuum vessel.

Melting of the Inconel proves that temperatures greater than 1350°C have been locally reached. The localization of the traces mainly on one edge of the contact area suggests that the tiles were tilted during the discharges. This means that the tiles were subjected to a torque greater than that produced by the clamping system force (150 N). Both phenomena can be caused by halo currents, the first because of joule heating in the contact resistance between tile and ring, the other due to the interaction between the current flowing in the tiles and the poloidal component of the magnetic field.

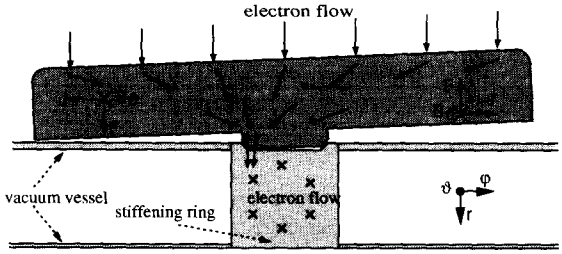

Fig. 5. Tilting force on the tiles due to halo currents.

A rough estimate can be made of the minimum current required to flow through a tile in order to tilt it as described in Fig. 5. With the maximum value of the poloidal component of the magnetic field (0.32 T), a minimum current of 2 kA has been deduced.

To estimate the current necessary to produce the observed melting, both experimental tests on prototypes of the first wall components and numerical analyses have been carried out. In order to measure the actual contact resistance between the graphite tiles and inconel rings and to validate the numerical analyses, impulsive tests with a duration comparable to an RFX discharge (100 ms) were performed on a tile-ring mock-up with an effective current of 3 kA. This current value was found to be sufficient to produce melting of the Inconel 625 in some concentrated spots. Transient thermal-electrical analyses were carried out by means of a finite element code [14] to determine the temperature distribution in the graphite tiles and Inconel 625 rings due to the joule heating of the electric current. The numerical results were in good agreement with the experiments and showed that a minimum current of 3 kA for a duration of 100 ms is necessary to raise the temperature in the contact region to over 1350°C.

The origin of halo currents in RFX can be ascribed to the effect of a radial displacement of the plasma column due to the magnetic field deformation induced by mode locking. The phenomenon is toroidally localized with an extension of approximately 1/10 of the major circumference, as derived by CCD camera images and magnetic measurements [7,15]. Unlike tokamak devices, where the poloidal component of a halo current is due to disruptive events [16], in RFX a large poloidal current in the outer part of the plasma column is always present, being necessary for the maintenance of the RFP configuration. Because of a radial deformation of the column, a particle flow can collide with the first wall and the current follows the path of the least electrical resistance in the structure, reasonably coming back into the plasma after about half a poloidal circumference in the vessel (Fig. 6).

A rough evaluation of the total halo current during a discharge can be made considering the toroidal and poloidal

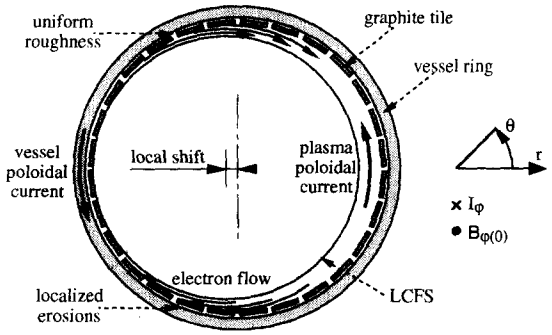

Fig. 6. Hypothetical halo current path in RFX.

extension of the plasma–wall interaction observed with the CCD cameras in the mode locking region. Assuming a current of 3 kA flowing in the vessel through 3 ÷ 4 tiles per stiffening ring and 5 rings, invested by the locked modes, a total halo current of approximately 50 kA is estimated. This value corresponds to about 10% of the toroidal current. Considering the electric resistance of the assumed path of the current in the structures, a total power dissipation of about 1.5 MW can be estimated, as a minimum reference value.

Typical RFP field profiles, assuming vanishing current density at the plasma edge, require a radial displacement larger than 10 cm to obtain the estimated total halo current. Recent measurements performed by an electron energy analyzer [17] have assessed non null current density in the RFX plasma edge. According to that, a lower radial displacement of a few centimetres is required, in agreement with the local magnetic shift measurements.

5. Conclusions

The investigation of RFX first wall and vessel after long term operation has revealed severe plasma wall interaction phenomena localized in the regions of the two poloidal gaps, where MHD modes preferentially lock in phase. The main damage is due to arc tracks and localized erosion at the edge of the graphite tiles, whereas grooves and uniform metal erosion take place in the metallic vessel. A strong redeposition is observed in proximity of the most eroded areas of the graphite tiles. The redeposition pattern on the rear side of the tiles has been related to the presence of a plasma flow, generated by the combined effects of the poloidal magnetic field and an ambipolar, outward directed, electric field. Traces of halo currents have been evidenced and related to the radial displacement of the plasma column due to the magnetic field deformation. Through thermal and electrodynamic stress analyses and CCD camera observations, the halo currents during a discharge have been evaluated to be approximately 50 kA, about 10% of the toroidal current, causing a power dissipation of about 1.5 MW.

References

[1] G. Rostagni, Fusion Eng. Des. 25(4) (1995) 301–313.
[2] F. Gnesotto et al., Fusion Eng. Des. 25(4) (1995) 335–372.
[3] V. Antoni et al., Plasma Phys. Controlled Fusion 35 (1993) B333–B342.
[4] V. Antoni et al., Proc. 15th Int. Conf. Plasma Phys. Controlled Nucl. Fusion Res. 2 (1994) 405–413.
[5] P. Fiorentin et al., Proc. 20th EPS Conf. Controlled Fusion and Plasma Phys. II (1993) 447–450.

[6] A. Buffa et al., Proc. 21st EPS Conf. Controlled Fusion and Plasma Phys. I (1994) 458–461.
[7] V. Antoni et al., Proc. 22nd EPS Conf. Controlled Fusion and Plasma Phys. 19c, part IV (1995) IV185–IV188.
[8] V. Antoni et al., J. Nucl. Mater. 220–222 (1995) 650–653.
[9] P. Sonato et al., J. Nucl. Mater. 227 (1996) 259–265.
[10] P. Wienhold et al., Nucl. Instr. Methods B 94 (1994) 503–510.
[11] L. Carraro et al., Proc. 22nd EPS Conf. Controlled Fusion and Plasma Phys. 19c, part II (1995) 11317–11320.
[12] V. Antoni, E. Martines, D. Desideri, G. Serianni and L. Tramontin, Nucl. Fusion, submitted.
[13] V. Antoni et al., Nucl. Fusion 36 (1996) 435.
[14] ANSYS User's Manual Theory rev. 5.1, Swanson Analysis System (1994).
[15] M. Valisa et al., these Proceedings, p. 988.
[16] F.C. Schuller, Plasma Phys. Controlled Fusion 37 (1995) A135–A162.
[17] Y. Yagi et al., presented at the 23rd EPS Conf. Controlled Fusion and Plasma Phys., Kiev, June (1996).